Single-channel basis for the slow activation of the repolarizing cardiac potassium current, I_{Ks}

Daniel Werry[1], Jodene Eldstrom[1], Zhuren Wang[1], and David Fedida[2]

Department of Anesthesiology, Pharmacology and Therapeutics, University of British Columbia, Vancouver, BC, Canada V6T 1Z3

Edited by Richard W. Aldrich, University of Texas at Austin, Austin, TX, and approved February 1, 2013 (received for review August 28, 2012)

Coassembly of potassium voltage-gated channel, KQT-like subfamily, member 1 (KCNQ1) with potassium voltage-gated channel, Isk-related family, member 1 (KCNE1) the delayed rectifier potassium channel I_{Ks}. Its slow activation is critically important for membrane repolarization and for abbreviating the cardiac action potential, especially during sympathetic activation and at high heart rates. Mutations in either gene can cause long QT syndrome, which can lead to fatal arrhythmias. To understand better the elementary behavior of this slowly activating channel complex, we quantitatively analyzed direct measurements of single-channel I_{Ks}. Single-channel recordings from transiently transfected mouse *ltk*$^-$ cells confirm a channel that has long latency periods to opening (1.67 ± 0.073 s at +60 mV) but that flickers rapidly between multiple open and closed states in non-deactivating bursts at positive membrane potentials. Channel activity is cyclic with periods of high activity followed by quiescence, leading to an overall open probability of only ∼0.15 after 4 s under our recording conditions. The mean single-channel conductance was determined to be 3.2 pS, but unlike any other known wild-type human potassium channel, long-lived subconductance levels coupled to activation are a key feature of both the activation and deactivation time courses of the conducting channel complex. Up to five conducting levels ranging from 0.13 to 0.66 pA could be identified in single-channel recordings at 60 mV. Fast closings and overt subconductance behavior of the wild-type I_{Ks} channel required modification of existing Markov models to include these features of channel behavior.

cardiac repolarization | potassium-channel gating | single-channel studies

The slow potassium current, I_{Ks}, functions late in the cardiac action potential to repolarize the membrane potential and provides a critical physiological reserve for abbreviating systole and allowing adequate ventricular filling at high heart rates (1–3). The I_{Ks} channel complex is formed by coassembly of the voltage-gated potassium (K_v) channel, KCNQ1 (K_v7.1), with the single transmembrane accessory subunit, KCNE1 (4, 5). The association of KCNE1 with KCNQ1 produces the slowly activating current waveform relevant to repolarization, because KCNQ1 alone activates within a few milliseconds at depolarized potentials. Underscoring the importance of this complex, mutations in either subunit can cause common forms of long QT syndrome, short QT syndrome, and atrial fibrillation (6–8) by altering the gating and/or expression of the channel complex.

Although the macroscopic biophysical properties of I_{Ks} are relatively well characterized, we still do not fully understand the basis for the slow activation of this important current, and we know very little about how this activation is effected by pore gating of the single-channel complex. Recent fluorescence studies of I_{Ks} voltage sensor movement have suggested that multiple voltage sensors must move before the KCNQ1/KCNE1 channel complex can conduct (9) and that this requirement both differentiates the complex from the pore-forming KCNQ1 subunit kinetics when expressed alone (9) and provides at least a partial explanation for the very slow activation of I_{Ks} currents. Single-channel studies on mutant *Shaker* (10) and K_v channels suggest that subconductance occupancy arising from heteromeric pore conformations also can slow the overall activation time course as a result of only partial opening of the pore (11). Preliminary evidence indicates that subconductance states play a role in the opening behavior of I_{Ks} channels, but the details and significance of these states are unknown (12).

Several groups have determined from noise variance analysis that KCNE1 either decreases (13) or increases the single-channel conductance of KCNQ1 three- to fivefold, but the reported conductance for I_{Ks} varies among these studies, in part because the rapid flicker activity of the channel complicates accurate measurements of variance (12, 14, 15). Yang and Sigworth (12) suggested a single-channel conductance, based on noise analysis at +50 mV, of 4.5 or 6.5 pS for human KCNQ1 expressed with human or rat KCNE1, respectively, in *Xenopus*. They noted that "unitary currents roughly 0.5 pA in size should be visible in single-channel recordings." From patches with three or more human I_{Ks} channels they observed rapidly flickering openings, the kinetics of which could not be characterized, and long first latencies to opening.

Pusch et al. (16) and others have suggested the presence of more than one open state with different open times for homomeric KCNQ1 channels and the I_{Ks} channel (3) or the presence of subconductance states (12). How subconductance states are involved in the opening and maintenance of I_{Ks} channel activity is unknown at present. Whether K_v channel pore-forming alpha subunits can contribute to subconductance independently or if subconductance arises from concerted conformational changes was addressed using a tandem dimer channel that linked mutant drk1 (K_v2.1) subunits with different activation thresholds (17). The highest prevalence of sublevels was observed at voltages expected to activate one set of subunits but not the other, and so it was concluded that subconductance levels arise from heteromeric pore conformations. Such a mechanism for subconductance is consistent with the observation of sublevels coupled to activation in the *Shaker* (10, 18) and K_v2.1 channel (11, 17). Therefore, the presence of sublevels in I_{Ks} may have important implications for the gating of this channel complex.

Here we provide answers to all the above questions. We have characterized single-channel recordings of human I_{Ks} and report on the conductance, open probability (Po), determinants of slow activation, and kinetics during bursts. In addition, we observe multiple, often long-lived, subconductance levels in the human I_{Ks} channel. The data emphasize the importance of the conductance substructure in determining the time course of I_{Ks} channel activation and therefore its physiological role during repolarization of the cardiac action potential. The data suggest that perhaps multiple subconductance levels are a common and important feature

Author contributions: J.E., Z.W., and D.F. designed research; D.W., J.E., and Z.W. performed research; D.W., J.E., and Z.W. analyzed data; and D.W., J.E., and D.F. wrote the paper.

The authors declare no conflict of interest.

This article is a PNAS Direct Submission.

[1]D.W., J.E., and Z.W. contributed equally to this work.

[2]To whom correspondence should be addressed. E-mail: fedida@interchange.ubc.ca.

See Author Summary on page 4170 (volume 110, number 11).

This article contains supporting information online at www.pnas.org/lookup/suppl/doi:10.1073/pnas.1214875110/-/DCSupplemental.

of K^+ channel activation, and the I_{Ks} channel complex provides a rare insight into this feature because of its uniquely slow activation time course. As such, these single-channel recordings of I_{Ks} give significant insight into the role of native channel pore opening in the general activation mechanisms of K^+ channels.

Results

Identification and Characterization of Single-Channel I_{Ks}. Our initial attempts to record single-channel activity that could be attributed to I_{Ks} were guided by our expectation of a low, single-digit, picoSiemen conductance assayed by noise analysis of multichannel patches recorded by Yang and Sigworth (12) as well as by the identification of a channel that slowly activates at positive membrane potentials. Under our transfection conditions approximately one in four patches contained activity that we attributed to I_{Ks}, and fewer of these contained only a single channel. This result supports previous speculation (12) that I_{Ks} channels cluster together at the cell surface, potentially making the study of single-channel behavior very difficult. In single-channel patches during repeated depolarizations, the I_{Ks} channel opened after a significant delay, with a mean (± SEM) first latency during 179 active sweeps of 1.67 ± 0.073 s at +60 mV (n = 5 patches). With few exceptions, the channel flickered rapidly in bursts for the remainder of the depolarizing pulse (Fig. 1*A*). Usually the channels opened first to a range of sublevels (0.1–0.25 pA) before reaching larger amplitudes of ∼0.5 pA (as discussed in more detail later). Upon repolarization to −40 mV, small outward step currents could be seen clearly (Fig. 1*A*, sweeps 3 and 9), as is consistent with a reversal potential more negative than −40 mV and in the range expected for the known potassium selectivity of I_{Ks} (19).

The combination of amplitude, flicker kinetics, outward tail current, and ensemble average behavior were used to differentiate I_{Ks} from endogenous channels, which generally displayed inward tail currents as well as larger amplitudes (>1.5 pA) and longer open times (>50 ms) with less flickering than I_{Ks} (Fig. S1).

The ensemble average of 100 sweeps from a single-channel patch exhibited macroscopic I_{Ks} kinetics, i.e., very slow current activation, lack of current saturation during continued depolarization, and a slowly deactivating tail current on repolarization (compare Fig. 1*B* with a macropatch from Fig. S2*A*). The small amplitude of the ensemble average current (maximum 0.06 pA) is a reflection of the large number (84) of silent sweeps without channel activity during the period of averaging in this patch, which was particularly quiescent for I_{Ks} activity.

Current amplitudes of idealized events collected from setting a single 50% threshold to opening resulted in at least two prominent peaks in the amplitude histogram, at ∼0.15 and 0.46 ± 0.006 pA at +60 mV (Fig. 1*C*). This level was found to be independent of the data filter frequency, up to 1 kHz (Fig. S3). Plotting the amplitude of the greater of these levels for several pulse potentials resulted in an amplitude–voltage relationship with a slope conductance of 3.2 pS (Fig. 1*D*).

Single I_{Ks} Channels Are Completely Inhibited by Chromanol 293B. As further confirmation that we were recording single-channel I_{Ks} activity, we used the selective I_{Ks} blocker, Chromanol 293B. Kinetic (20) and structural (21) studies suggest that Chromanol 293B is an open-channel blocker that binds to the I_{Ks} inner pore vestibule and the lower part of the selectivity filter, making it necessary for the compound to enter from the intracellular side. Indeed, 50 μM bath-applied Chromanol 293B (IC_{50} of ∼5 μM; ref. 22) was able to inhibit completely a macropatch current externally isolated from the bath solution by the pipette tip (Fig. S2*A*). Before block, the current showed clear I_{Ks} kinetics resulting from the presence of tens of channels. Similarly, 50 μM

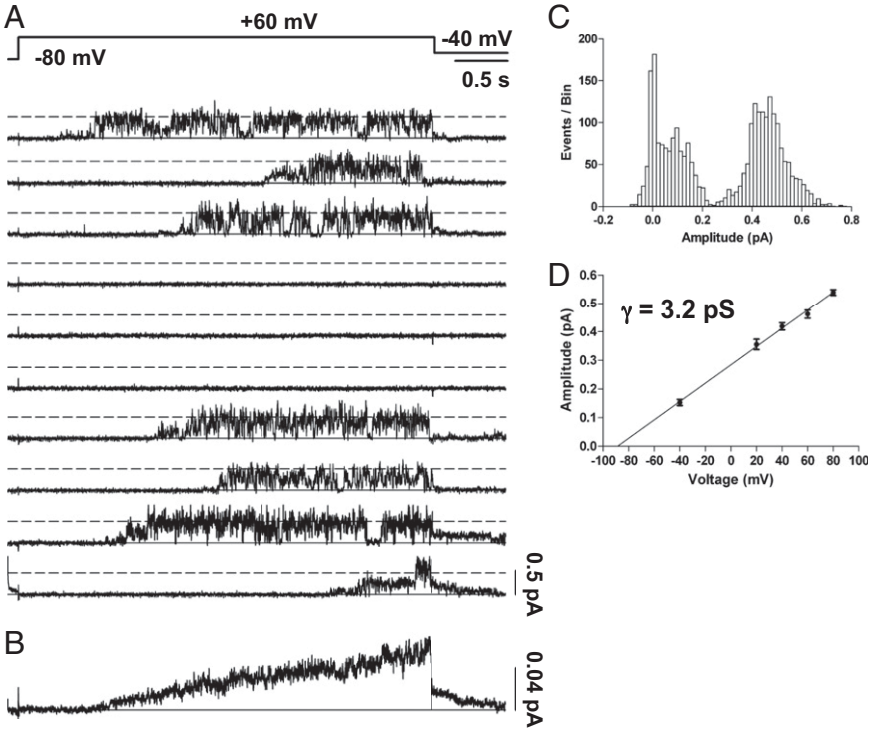

Fig. 1. Single-channel recordings of I_{Ks}. (*A*) Membrane patch containing a single I_{Ks} channel was stepped from −80 to +60 mV for 4 s and then to −40 mV for 0.75 s as indicated in the protocol at top. Shown are 10 of 100 sweeps from a cell-attached patch. (*B*) All 100 sweeps from the cell in *A* were averaged to yield the ensemble current, which has clear I_{Ks} activation and deactivation kinetics. (*C*) Idealization of the records by setting a single 50% threshold for opening yielded an amplitude histogram with a mean open amplitude of 0.46 ± 0.006 pA and a smaller amplitude of ∼0.15 pA. (*D*) Mean open amplitudes for several voltages were plotted and fitted linearly with a slope conductance of 3.2 pS and an extrapolated reversal potential consistent with potassium selectivity. $n \geq 3$ patches for each voltage.

Chromanol 293B completely inhibited I_{Ks} single-channel activity within seconds of bath application (Fig. S2*B*). We used a concentration (50 μM) expected to abolish I_{Ks} channel activity completely, because a partial, rapid open-channel block would be difficult to distinguish from a decrease in Po at the single-channel level.

Voltage and Time Dependence of Single-Channel Po. Like all K_v channels, the Po of I_{Ks} is coupled tightly to transmembrane voltage. Multiple factors, including temperature, β-adrenergic stimulation, and KCNE1 stoichiometry, affect the voltage dependence of I_{Ks} opening (23, 24). Under our recording conditions of room temperature, no exogenous β-adrenergic stimulation, and DNA concentrations producing an expression level of KCNE1 that saturate KCNQ1 (25), we expected large depolarizations to be required for single-channel I_{Ks} activation, consistent with other studies (12, 24). This appeared to be the case, because the original data showed few, if any, channel openings at 0 mV (Fig. 2*A*). We measured the sweep-averaged Po from idealized waveforms at 100-ms time intervals during 4-s pulses to different depolarizing voltages (Fig. 2 *A* and *B*). A single Boltzmann function fitted to the mean Po after 4 s versus voltage yielded a half-maximal voltage for the Po of +47 mV (Fig. 2C). In representative patches, the average Po at +60 mV reached ~0.15 after 4 s and showed no consistent signs of saturating (Fig. 2*B*). Although a Po of 0.15 at 4 s seems quite low, it is consistent with a steady rise in the macroscopic I_{Ks} well beyond 4 s (26). Over the course of 100 sweeps at +60 mV for 4 s, many successive sweeps typically had limited channel activity (Fig. 2*D*). Interestingly, active sweeps were clustered together, separated by long periods of quiescence. This wax-and-wane phenomenon also was observed in I_{Ks} with rat KCNE1 (12), but the physiological importance of this cyclic activity is not known.

Long First Latencies to Opening Partially Account for Slow Macroscopic Current Activation. In active sweeps, the channels opened after long latencies (typically 1–3 s) at +60 mV (Fig. 3*A*). The stepwise cumulative latency distribution scaled by a factor of 0.75 superimposed reasonably well with the ensemble time course of Po (noisy trace, Fig. 3*B*), indicating that once the channel opens, it has a high chance of staying open. When we take into consideration that the Po during bursts is less than 1 because of brief visits to closed states, the probability of the burst continuing to the end of the depolarizing pulse is higher than 75%. For one set of data, this value was measured at 77% for all 23 active sweeps and at 85% if we did not include the two sweeps (2 and 8) that contained few events and never opened beyond smaller subconductance levels. The initial rising phase of the ensemble Po (1–2 s; Fig. 3*B*) lies above the scaled latency distribution, suggesting that sublevel contribution to early activation was not picked up in our single-threshold idealization analysis to determine first latency. Analysis of one set of data using a half-amplitude criterion resulted in an average first latency of 1.92 ± 0.98 s but was 1.65 ± 0.96 s when five subconductance states were considered. Beyond the initial rising phase, the cumulative latency distribution fits well with the ensemble time course. Thus, long latencies to the first channel opening are an important determinant of the delayed initial I_{Ks} activation, but the rising current time course then is determined critically by the progression of activating channels through open subconductance levels.

Multiple Open and Closed States Are Visited During Bursts. Upon opening, the channels flickered rapidly between open and closed levels, measured using a 50% amplitude criterion. Closed-event durations grouped in 1-ms bins were consistently best fit with fast (C_f), intermediate (C_i), and slow (C_s) components, corresponding to mean time constants of 1.3 ± 0.3 ms, 7.1 ± 0.8 ms, and 50.9 ± 9.0 ms, respectively (Fig. 3*C*). Rare occurrences of longer

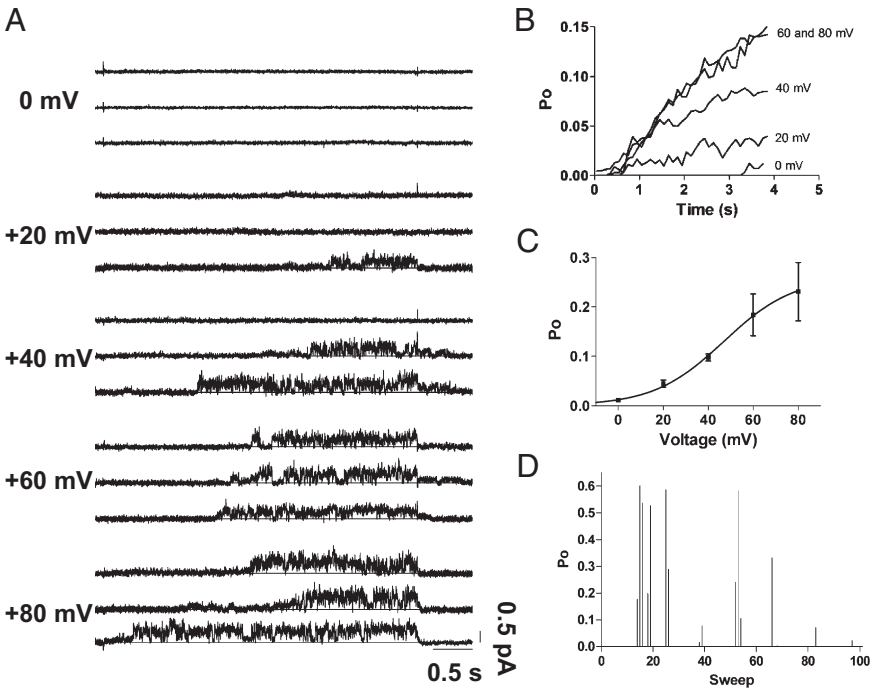

Fig. 2. Single-channel Po versus voltage. (*A*) Three representative traces for each indicated voltage from single-channel patches demonstrate increased single-channel activity with depolarization. (*B*) After idealization, the sweep-averaged Po of a representative patch at each voltage was plotted versus time during the depolarizing pulse. (*C*) The mean Po values at the end of each depolarizing voltage step were fit with a single Boltzmann function to give a voltage of half-maximal Po of +47 mV (n = 2–4, except at 0 mV). (*D*) Diary plot of the time-averaged Po during 4-s depolarizations to +60 mV. Po values of zero correspond to sweeps with no activity. Active periods tend to cluster and can be separated by long periods of no activity. Active sweeps reached a mean Po of nearly 0.6.

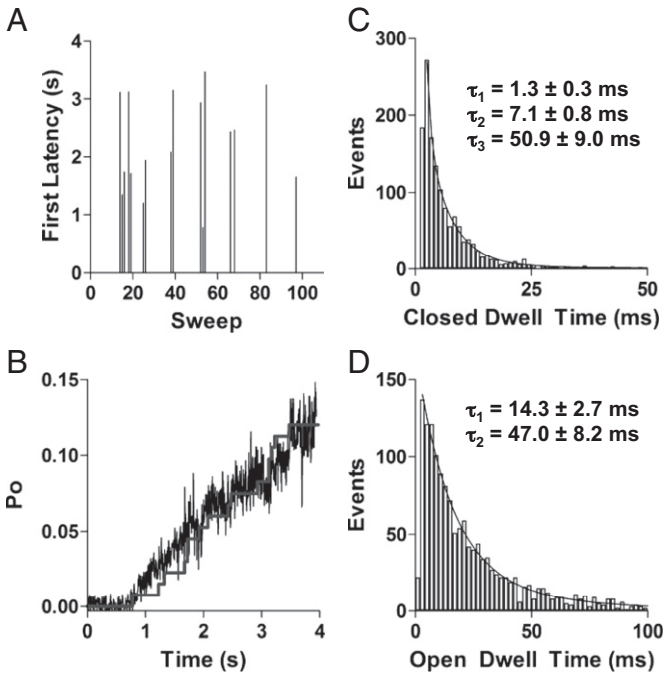

Fig. 3. Kinetics of single I_{Ks} channel opening and closing. (*A*) Representative diary plot of first latency to opening during 4-s depolarizations to +60 mV. Latency values of zero correspond to sweeps with no channel openings. (*B*) The ensemble mean time course of Po at +60 mV (noisy trace), calculated by dividing the ensemble average of 100 sweeps of single-channel currents by the mean open amplitude of the largest level (0.46 pA). The superimposed stepwise curve is the first latency distribution, scaled by a factor of 0.75. All data from *A* and *B* are from the same patch. (*C*) Closed event dwell times were binned in 1-ms intervals and fit with three exponential components, giving the mean time constants shown. (*D*) Open dwell-time histograms were binned in 2-ms intervals and best fit with two exponential components, giving mean time constants shown.

closings were observed (e.g., 137 ms for sweep 9 in Fig. 1*A*) but were too few for analysis. Although infrequently visited, the C_s state can be seen in the recordings as shorter interruptions in burst activity (e.g., sweep 8 in Fig. 1*A*), whereas the C_i and C_f states occur within the bursts (Fig. 1*A*). The C_f state was the most frequently visited closed state and was a major contributor to the rapid flickering seen in the recordings (Fig. 1*A*). Open events were best fit with two exponential components which yielded mean time constants of 14.3 ± 2.7 ms and 47.0 ± 8.2 ms at 60 mV (Fig. 3*D*). Given a dead time of 0.9 ms for a 200-Hz, 3-dB filter, many of the very brief C_f events went undetected, potentially leading to an overestimation in the mean open dwell times or to the failure to detect another component of the open-time distribution (27). However, low-pass filtering at 200 Hz was deemed necessary to avoid detecting false events, given the signal-to-noise ratio for much of our data. Rapid transitions between subconductance open states also appear to contribute to the rapid flicker appearance of I_{Ks} activity during bursts, as described next.

I_{Ks} Has Multiple Subconductance Levels. Although the often-used 50% amplitude criterion is convenient for a basic analysis of the opening and closing kinetics of I_{Ks}, as described in Fig. 3, it is inadequate to explain the behavioral complexity of the open pore in the single I_{Ks} channel complex. The I_{Ks} channel nearly always enters long-lasting subconductance levels before reaching the fully open amplitude. This phenomenon is clearly observable in the records (Figs. 1*A* and 4*A*) and in the shape of the all-points histogram (Fig. 4*C*). A channel can be seen to dwell in multiple levels for prolonged periods during its initial activation (Fig. 4*A*), with sublevels visited briefly and interspersed by rapid switching between open and closed levels, as previously seen in Kv channels (11). The mean time to reach the main amplitude (level 4) from the start of each sublevel opening burst was 209 ± 46 ms (n = 21 bursts), excluding two bursts where the channel opened to levels >4 for brief periods and then closed for ~750 and 1,460 ms, respectively, before reopening and subsequently attaining the main conductance level. Interestingly, mean dwell times at level 1 before the channel reaches the main conductance level are longer (13.6 ± 1.52 ms) than the mean times for the remainder of the burst (4.08 ± 0.25 ms).

Once the main open amplitude is reached, the channel continues to fluctuate between multiple levels. From the main level 4, transitions can be seen to three lower substates and a closed level as well as less frequently to a fifth open level (0.66 pA) that actually is higher than the main open amplitude (Fig. 4 *A* and *C*). The phenomenon of multiple open levels also is apparent during channel deactivation upon repolarization (Fig. 4*B*). To support the idea of distinct conductance levels, we constructed all-points amplitude histograms from raw data, filtered at 200 Hz (corner frequency, *fc*). All-points histograms are limited in their capacity to distinguish conductance levels because of overlapping noise and points detected during transitions (28), but evidence from this analysis for up to five peaks was confirmed after idealization of data from multiple different patches (e.g., Fig. 4 *C* and *D*). We approached the selection of putative levels by observing the levels of clear long-lived events and/or by identifying the peak of the all-points histogram and applying the "3/2 rule" (29) to derive the other levels. Open levels 3 and 4 gave the most prominent peaks, with level 3 being visited most often and level 4 being visited for longer times. The total dwell times at each level for all sweeps (n = 97) in the dataset in Fig. 4*D* were 346 s (closed state); 4.32 s (0.13 pA); 4.0 s (0.196 pA); 8.4 s (0.293 pA); 17.2 s (0.44 pA); and 6.17 s (0.66 pA).

The mean (±SEM) dwell times in the main conductance level 4 (0.44 pA) and level 5 (0.66 pA) were longer: 5.99 ± 0.39 ms (level 1); 4.13 ± 0.18 ms (level 2); 6.52 ± 0.22 ms (level 3); 13.7 ± 0.48 ms (level 4); and 14.6 ± 1.25 ms (level 5) (Table S1).

As an additional, more objective mechanism for estimating the substate current amplitudes, we also used the procedure typically used by the developers of the QuB software. That is we first used the "Amps" function of QuB, which uses a Baum–Welch algorithm to estimate amplitudes of each conductance class (www.qub.buffalo.edu/wiki/index.php/Modeling:Amps), then "Idealize" using the segmental k-means (SKM) method (30). The resultant amplitudes in pA (±SD) were 0.00160 ± 0.02582 (closed state); 0.08243 ± 0.02834 (substate 1); 0.18704 ± 0.03505 (substate 2); 0.30915 ± 0.03576 (substate 3); 0.45087 ± 0.05309 (substate 4); and (substate 5) 0.65538 ± 0.08617 (substate 5). These numbers are very close to our own with the exception of the somewhat lower first substate. Given the small amplitude of this substate, we expected that it would be the most difficult to discern among the noise, and indeed the average was brought down by estimations on two segments of 0.055 pA and 0.043 pA. Removal of these values resulted in a first substate amplitude of 0.09556 ± 0.01241 pA.

Single-Channel Activity in an I_{Ks} Mutant with High Po. Because the Po of WT I_{Ks} channels is so low (~0.12 after 4 s; Fig. 3*B*), it can be difficult to discern the exact number of channels in a cell-attached patch. Thus, it is important to establish that the current sublevels described above are indeed subconductance levels rather than four or five channels present in the patches. Altogether we obtained eight patches in which the maximum single-channel current level at +60 mV was 0.46 pA and no patches with I_{Ks}-like activity that had smaller maximum current levels. This result suggested that 0.46 pA is about the lower limit for the single-channel current at this potential.

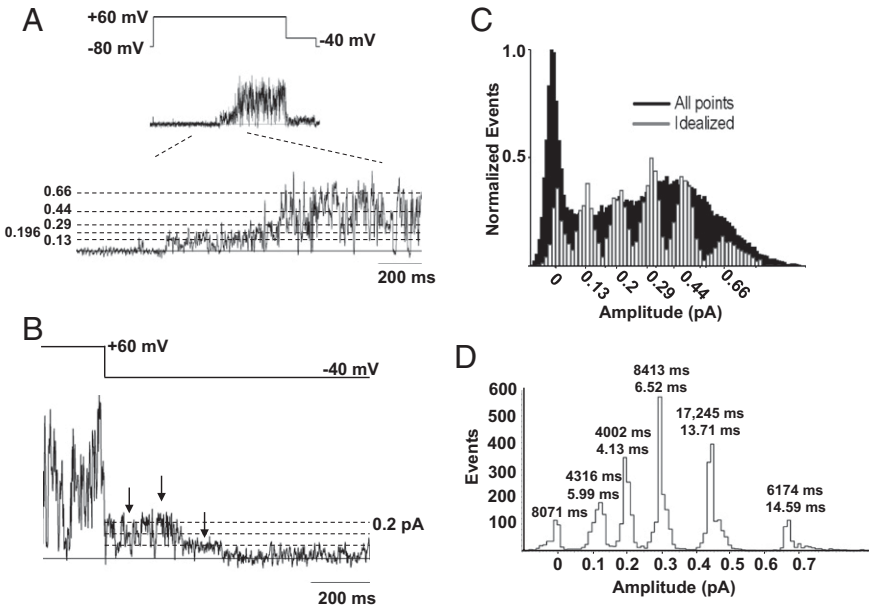

Fig. 4. I_{Ks} shows multiple subconductance levels during bursts of activity. (*A*) Single-channel current during voltage pulse illustrated by protocol at top. An expanded section of the current record is drawn below, and putative opening levels are shown by the dotted lines. (*B*) A second current trace, highlighted during the repolarization step to −40 mV, illustrates at least three putative subconductance levels, as indicated by arrows. (*C*) All-points amplitude histogram (black; filtered at 1,000 Hz) obtained from a single 4-s current trace during a +60 mV step. The superimposed amplitude histogram (white) was constructed from events idealized by setting five separate thresholds corresponding to the amplitudes shown and is from data filtered at 200 Hz. (*D*) Amplitude histogram from a second single-channel patch analyzed using a five-open amplitude criterion. Twenty-three active sweeps out of a total of 97 sweeps during 4-s voltage steps to +60 mV were analyzed. The times above each peak are the total and mean dwell times in each sublevel.

However, we felt that a much better way to show directly that the single-channel amplitude at full opening is ~0.5 pA at +60 mV was to make single-channel recordings from a gating mutant of I_{Ks} that we previously have shown (25) to have a much higher Po than WT channels. The whole-cell findings from the S209F mutant are summarized in Fig. S4*B* (compare with WT I_{Ks} in Fig. S4*A*) and showed a negative shift of activation gating of ~60 mV and a Po of 0.4 at −50 mV that gave sustained tail currents and highlighted the increased Po of the mutant channel. Because the channels are open so much of the time in this mutant, if there were more than one channel in a patch we would expect to see discrete steps in channel amplitude, which we did not. As shown

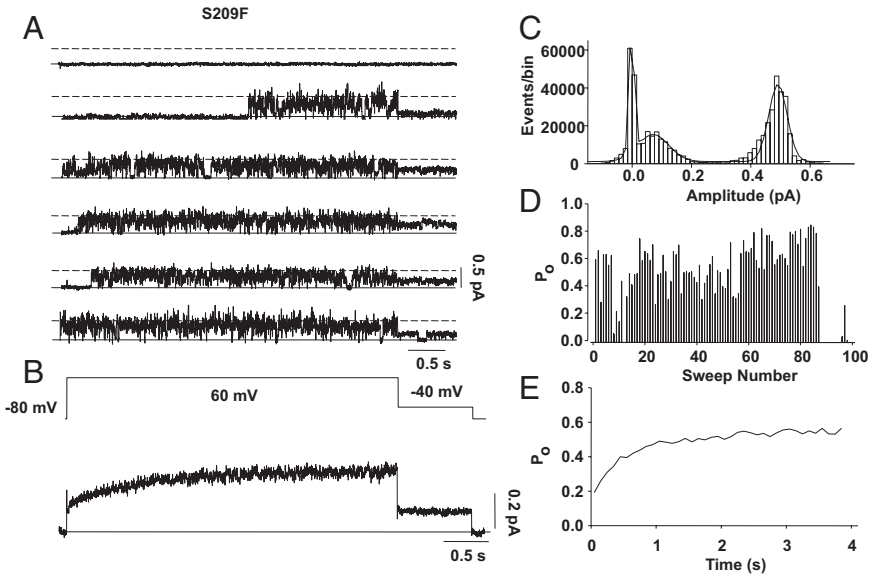

Fig. 5. Single-channel patch data of the gain-of-function I_{Ks}-S209F mutant. (*A*) Single-channel sweeps for 4 s to +60 mV show opening of a single channel throughout almost the entire 4-s pulse, usually opening after a short latency. Note that in sweep 1 the channel remains closed. The solid line indicates zero current. (*B*) Ensemble average current for 67 current recordings shows rapid activation of I_{Ks} and sustained current on repolarization to −40 mV. (*C*) Histogram of idealized event amplitudes. Note that because of high Po, events are dominated by the fully open level at +60 mV (I = 0.43 ± 0.03 pA). (*D*) Po during 100 sweeps of train shows the high opening frequency of the channel. (*E*) Ensemble-averaged Po from 100 successive sweeps during 4-s depolarizing pulses to 60 mV.

in Fig. 5*A*, the channels did not invariably open at +60 mV, but when they did the dominant opening of the channel was at a level close to 0.45 pA in more than 40,000 events in 200 sweeps for this particular single channel (Fig. 5*C*). As shown in the diary plot in Fig. 5*D*, at +60 mV this channel had periods of silence followed by periods of very high activity, giving an overall Po of ~0.6 (Fig. 5*E*), about five times that of WT (Figs. 2*D* and 3*B*). The ensemble average of single-channel currents had an instantaneous component to activation and exhibited little sigmoidicity (Fig. 5*B*). Upon repolarization to −40 mV, the channels continued to flicker, showing little sign of deactivation over 750 ms (Fig. 5 *A* and *B*). The very slow deactivation of this channel at −40 mV suggests that the channel is stabilized in the open conformation at this potential, similar to other gain-of-function mutations described in KCNQ1 (31). The shorter component of open dwell times was twice as long as in WT (25.9 ± 5.0 ms vs. 14.3 ± 2.7 ms), and the longer component to opening was about 1.5 times as long (69.9 ± 4.8 vs. 47.0 ± 8.2 ms), confirming this hypothesis.

The full dataset from the S209F mutant had a single-channel conductance of 3.18 pS (n = 16), very close to the WT conductance, and recordings from a patch containing two channels exemplify this similarity (Fig. S5). Here, clear peaks in the all-points histograms are seen at the 0.45 and 0.91 pA levels. Also, during tail steps to –40 mV two clear opening levels are seen at 0.22 and 0.41 pA (Fig. S5 *B* and *D*). These levels give a calculated conductance of 3.4 pS for this particular patch. We did not observe sustained opening to lower levels (as would be expected if the single-channel conductance were lower than 3 pS) in any S209F patches from which we obtained recordings.

Subconductance Latencies During Activation. To understand more about the interrelationships between subconductance states during activation, we measured the first latency to opening for each of the five putative sublevels. Sublevels arising from partial activation of the channel would be expected to occur before fully open levels. Indeed, the probability distribution of cumulative latency indicated that the first latency of a given level is correlated with the amplitude of the level (Fig. 6*A*). The results suggested that most of the latency before channel opening reflected a gating delay before any pore opening and that the subsequent pore opening occurred through sublevels in a sequential fashion. We hypothesize that sublevels may be coupled to deactivation as well, because there was evidence that at least two sublevels were traversed en route to full channel closure during single-channel tail currents at −40 mV (Fig. 4*B*).

We already have shown (Fig. 4) that once channels reach a certain open sublevel, they may close and reopen rapidly, at a much faster rate than expected from the sublevel latency distributions just described (Fig. 6*A*). This rapid closing and reopening suggests that I_{Ks} sublevel closings within bursts are not traversed as part of the normal channel activation pathway but rather represent C_f states in parallel with the open states and outside the activation pathway, as suggested from the kinetic analysis presented in Fig. 3 and as described for *Shaker* B channels by Hoshi et al. (32). The data in Fig. 6 *B* and *C* illustrate transitions between these subconductance states and the closed state. The data show that channels can close from one subconductance level and reopen at the same level (Fig. 6*B*) or at another open level (Fig. 6*C*). This analysis is limited by the dead time of the system of 0.11 ms at a corner frequency of 1 kHz used in Fig. 6 but nevertheless demonstrates the existence of multiple C_f states in parallel with the subconductance states (see below).

Model of Single-Channel Activity. To place our data in the context of gating schemes, we used a well-recognized model of macroscopic I_{Ks} complex currents (3) as the basis for modeling single-channel activity. Other, recent, allosteric models have been proposed for the KCNQ1 alpha-subunit of the I_{Ks} complex alone (33, 34), and these have been used mainly to model activation curve position and slope in WT and mutant channels. However, our preliminary investigations demonstrated that such models cannot easily reproduce the long latencies to opening seen in the I_{Ks} experimental data and also simulate the rapid transitions between channel substates and closed states during bursts of opening activity.

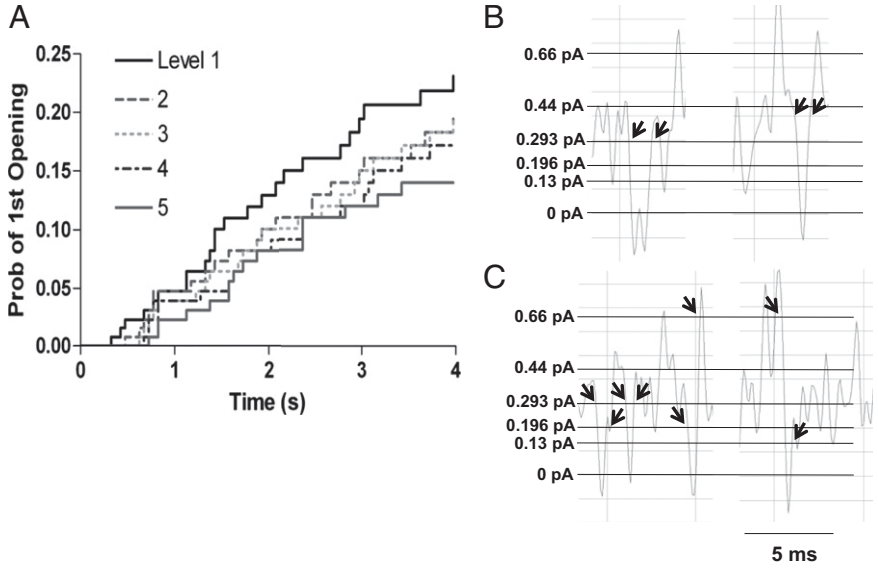

Fig. 6. Probability distribution for each of five putative levels and closer examination of level transitions. (*A*) Cumulative first latency probability distribution for each of five putative levels from 100 current traces from a single-channel patch during steps to +60 mV. The smallest conductance level (level 1) occurs earliest, followed by each larger level in turn. (*B*) Examples of closing events that returned to the same conductance level after reopening. (*C*) Examples of closings where the channel reopened to different amplitudes as indicated by arrows. Filtering for *B* and *C* was at 1 kHz. Data were obtained from sections of the single-channel current record during steps to +60 mV.

The Silva–Rudy model (3) reproduces latencies to first openings very well for our data and allowed us to concentrate on the activation steps during pore opening itself. Because our interest was to gain insight into the real-time opening and closing data that we have collected, no changes have been made to the rates in the activation range and in preopen states except for the final closed-to-open transition in the Silva–Rudy model (Fig. S6). Given the difficulty in analyzing the fast, multilevel gating behavior of I_{Ks}, our intent was not so much to determine the rates accurately but rather to broaden the model to account for additional features, i.e., the existence of multiple sublevels and the "flicker" behavior resulting from both the rapid movement between sublevels and fast closings.

Our modified form of the model to account for single-channel behavior is shown in Fig. 7*A*. Activation in the Silva–Rudy model incorporates four independent subunits undergoing two allosteric transitions to opening, as shown and as based on the work of Hoshi et al. (32). In our modification, for the pore to conduct, all subunits must undergo at least the first transition (open triangles), and at least one subunit must have undergone the opening transition (open circles). Thus, all those states within the shaded box are able to conduct ions, with conductances proportional to the number of activated subunits. We also have reported that rapid closings during bursts of channel activity are not in the activation pathway, so that multiple rapid C_f states are shown in parallel with the open substates. Data show that channels that rapidly close from different substate levels during the bursts of activity may or may not reopen to the same substate (Fig. 6). Thus, the C_f channel states are vertically coupled.

The inclusion of the subconducting states allowed us to reproduce accurately the kinetics of I_{Ks} single channels during depolarizations to +60 mV and during deactivation at −40 mV (Fig. 7 *B* and *C*). Channels first open after long latencies (1.75 ± 0.016 s) and usually open to subconductance levels before reaching the fully open states. Deactivation shows the closing of the channel and also shows occupancy of subconductance states during deactivation. In the lower panel of Fig. 7*B* the ensemble average of model single-channel current recordings (black) overlays the experimentally obtained ensemble average (red), reproducing the current activation time course accurately.

We found that allowing larger and equal forward rates between the sublevels, as well as equal reverse rates (Fig. S6), allowed the channel to move freely between substates rather than accumulating in the final open state. Nonetheless, the relative occupancy of the open substates indicates that the "main" open state, indicated by the asterisk in Fig. 7*A*, still has the highest occupancy, as was found experimentally (Fig. 4 *C* and *D*), perhaps because there are fewer pathways for exiting this state. Open and closed time distributions were calculated from 50 model runs that then were analyzed using the half-amplitude criterion in Clampfit 10 (Fig. 7 *D* and *E*). Open and closed times were fit with three and two exponential functions, respectively, and matched experimental data well (Fig. 3).

Discussion

Quantitatively, our data show that the fully open I_{Ks} channel level is reached via multiple subconductance levels in the WT channels and the fully open channel conductance is close to 3 pS,

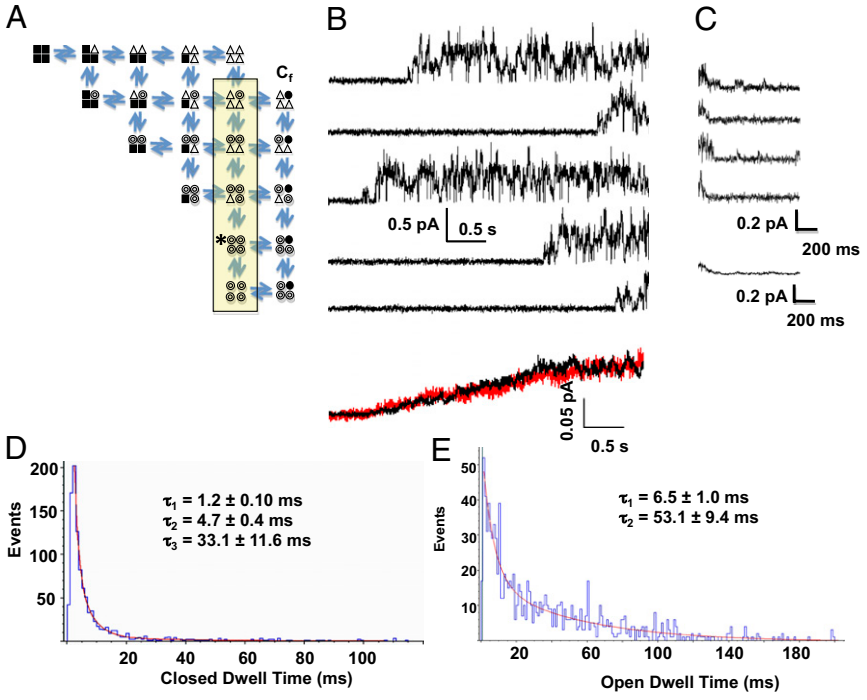

Fig. 7. I_{Ks} Markov model and simulated data. (*A*) The 21-state model used to simulate I_{Ks} currents. The states within the yellow box are all conducting, with increasing current amplitude from top to bottom, based on experimental data. Filled squares represent subunits in their resting conformation; open triangles are those that have undergone the first activating transition; open circles are those that have undergone the second activating transition and have become conducting. The C_f closed states to the right of the conducting states represent fast closings that are outside the direct activation pathway. (*B*) Data generated by the model using QuB software. Each of the top five traces simulates a 4-s sweep of single I_{Ks} channel activity, and the final trace is an ensemble average of 98 simulated sweeps (black trace), of which 23 were active sweeps and 75 were blank, similar to the activity observed in experimental data (red trace). (*C*) Simulated deactivation data, with rates calculated for a membrane potential of −40 mV and the main conducting level designated as the starting state (indicated with an asterisk in *A*). The bottom trace is an ensemble average of five traces. (*D*) Closed-event distribution from 50 simulated sweeps binned in 1-ms intervals according to dwell time and fit with three exponential components, giving the mean time constants shown. (*E*) Open dwell-time distribution from the 50 traces of simulated data were best fit with two exponential components, giving the mean time constants shown.

a finding that is supported by data from the S209F I_{Ks} mutant channel, which has a very high Po during active sweeps.

Kinetic Properties of Single Channel IKs. These single-channel recordings of I_{Ks} reveal the stochastic behavior underlying the macroscopic current. The data show that the well-recognized slow activation of I_{Ks} is caused in part by single channels showing very long latencies to first opening to the first subconductance level (Figs. 1 and 3*A*). Full opening itself is delayed further by the occupancy of partially open subconductance states before channels reach the fully open state (Figs. 4 and 6*A*). Transition between sublevels also is relatively slow, so that it can take >100 ms longer for the channel to reach the main conductance level after initially opening to the first level (Fig. 6*A*).

Once channels open, they burst fairly continuously, rarely deactivating until repolarized (Fig. 1*A*). Periods of quiescence giving silent sweeps between sweeps of bursting activity underlie the low overall Po (Figs. 2*D* and 3*A*) and suggest that channels can enter dormant states that render them particularly resistant to activation. If dormant states reflect an early closed state in the activation pathway, two slow transitions are needed to explain this behavior, one to account for the seconds needed for the channel to activate ordinarily and another, even slower, transition to account for the sometimes long dormant periods that can last many minutes. Alternatively, the long dormant state we observe may not be part of the linear activation pathway but instead may be an alternative gating mode of the channel, similar to that seen for sodium (35) and calcium (36) channels, and may be influenced by turnover of molecules that modulate I_{Ks} activity, such as Phosphatidylinositol 4,5-bisphosphate (PIP2), ATP, PKA, or calmodulin (37–40). It is likely that channels can be recruited from dormant to active states in the face of sympathetic activation when I_{Ks} function becomes most prominent, but this possibility remains to be proven (38, 41).

Slow entry into and exit from bursts confers the slow activation and deactivation properties of I_{Ks}, respectively, but the intraburst gating of the channel is rapid. The rapid flickering during bursts complicates a precise dissection of open and closed states and may cause truncation of high-frequency components, as previously determined by a dependency of variance (and thus single-channel amplitude) on bandwidth for I_{Ks} (12, 14). However, we found the main level amplitude to be independent of bandwidth over a range of 200–1,000 Hz (Fig. S3). The main open level peaks in all-points histograms constructed from raw data filtered at 200 and 1,000 Hz overlapped closely, supporting our estimate of a fully open channel conductance of 3.2 pS (Fig. 1*D*).

Distributions of closed dwell times during bursts were best fit with three exponential components (Fig. 3*C*), similar to the C_f, C_i, and C_s closed states described in the *Shaker* channel (32, 42). It is clear, with the channel able to open and close from all substates, and from our modeling, that at least the C_f state visited during I_{Ks} flickering lies adjacent to the activation and deactivation pathways and not in the pathway to first opening. The structural mechanism for fast closures during bursts may be related to subtle conformational changes with low energetic barriers and/or ion dwelling at the selectivity filter (43). Open dwell times were best fit with two exponential components (Fig. 3*D*), but we cannot conclude from this result that there are only two kinetically distinct open states, because this kinetic analysis was performed by setting a single 50% threshold to opening, which groups open levels together (sublevels below the threshold were ignored in this analysis). Because our more detailed analysis of subconductance levels in Fig. 4 demonstrated the presence of five sublevels, the longer open dwell-time component ($t = 47.0 \pm 8.2$ ms) may reflect transitions through multiple open levels before a closure was detected, whereas the shorter component ($t = 14.3 \pm 2.7$ ms) may reflect a single open level. It is likely that rapid transitions between open substates contribute to the rapid flicker appearance of I_{Ks} activity during bursts. Still, these kinetic values obtained for the I_{Ks} channel provide information not previously available.

Substates of the Open I_{Ks} Channel. Both long-lived and short-lived sublevels were seen commonly during I_{Ks} activity (Figs. 1 and 4). A potential mechanistic basis for subconductance levels involves limited cooperativity between pore-forming subunits (44), which enables some, but not all, of the subunits to reach a conducting conformation (17) at a lower conductance. Subconductance levels have been observed in a variety of channels (45) and may be a feature of all K_v channels. In the *Shaker* channel, subconductance levels presented themselves in single-channel recordings as brief shoulders traversed during transitions to a full open level (10). In contrast, sublevels in I_{Ks} often persisted for hundreds of milliseconds before entering larger conductance open states (Figs. 1*A*, 4*A*, and 6*A*). A possible explanation for this persistence is that I_{Ks} subunits exhibit relatively low cooperativity, so that activation of one subunit only weakly promotes activation of other subunits, hence the equal rates in the model for the substate transitions. The final steps of the I_{Ks} activation pathway then are slow enough to reveal stable sublevels, as was the case in a slow mutant of $K_v2.1$ (11). If so, KCNE1 may slow I_{Ks} activation by promoting sublevel stability through as yet undetermined mechanisms. The long-lived sublevels occurred primarily before full opening, suggesting that these sublevels are coupled to the activation pathway and that at least some allosterism occurs once bursts of activity are fully established, because dwell times in open level 1 are then reduced.

Up to five conductance levels can be rationalized in a tetrameric channel if the number and arrangement of activated subunits determines the conductance (Fig. 7*A*) (11). The arrangement of activated subunits may be important in the case of two active subunits that are either adjacent to or opposite each other (11, 18). An integral feature of a subunit-based mechanism of subconductance is that smaller sublevels (resulting from fewer activated subunits) are predicted to occur earlier in the activation pathway (11, 18). Indeed, in I_{Ks} channels, the larger conductance levels had longer latencies to first opening (Fig. 6*A*), and the smallest subconductance level was traversed at least 75% of the time before larger open levels were reached. We suspect that subconductance levels occasionally were traversed too quickly to be detected in the analysis. Therefore, our observations of subconductance levels in I_{Ks} are consistent with a subunit-based mechanism, whereby sublevel states are traversed through the activation pathway en route to full conductance. The presence of activation-coupled sublevels in I_{Ks} argues against a single, concerted transition to full opening for this channel and argues in favor of stepwise transitions of each subunit.

Sublevels were much longer lived before the channel reached larger open levels than after. Therefore, we hypothesize that the stability of a sublevel is dependent on the activation state of the nonconducting subunits. After large open levels are reached, all the subunits are either in open conformations or in closed states near opening, so the channel dwells only briefly at the subconductance level when it is revisited in the same burst. Efforts to place subconductance levels into a canonical gating scheme of two transitions per subunit (46) have differed in whether they assume that all four subunits must undergo the first transition, commonly interpreted as voltage sensor movement, before a single subunit can become permissive to ions (11, 18). That all four voltage sensors must move before the I_{Ks} channel can open has been suggested recently from fluorescence reports of KCNQ1 S4 movement when in complex with KCNE1 (9). With the first transition as a prerequisite to opening, a scheme with two transitions per subunit limits sublevels to single kinetic states with nonopen subunits restricted to an intermediate state between resting and conducting. However, the dependence of I_{Ks}

sublevel stability on the activation state of the channel suggests that the nonconducting subunits are not constrained to single states during subconductance. Therefore, an additional transition to opening might be necessary to explain this behavior. A model with three transitions per subunit was proposed previously to account for kinetic phenomena at voltage extremes in the *Shaker* channel (42, 47).

Single-channel recordings of I_{Ks} are an important step toward understanding the stochastic behavior of this channel complex and open the door for many future studies. For example, the mechanistic basis for increases in macroscopic current by modulators such as PKA (38) and PIP2 (37, 48) now can be studied at the molecular level. It is interesting to speculate whether conductance-level occupancy is a target of modulation. Furthermore, the structural basis for subconductance levels has yet to be determined. Although individual movements of subunits at the activation gate have been shown in KcsA (44), altered ion selectivity for subconductance levels in *Shaker* implicates conformational changes around the selectivity filter (10). It would be of great interest to test if subconductance levels in I_{Ks} display different selectivity for permeating ions such as rubidium. If so, the differential selectivity may explain the relatively low potassium selectivity of I_{Ks} compared with other K_v channels (19).

Methods

Cell Preparation and Transfection. Electrophysiology was carried out on transiently transfected mouse *ltk-* cells plated onto sterile glass coverslips at 20–30% confluence and grown in minimum essential media with 10% FBS at 37 °C in an air/5% CO_2 incubator. *KCNQ1* and *KCNE1* genes were purchased from Origene Technologies. DNA ratios (in micrograms) of 1:2.5:1 of *KCNQ1 (*or *KCNQ1*-S209F):*KCNE1:*GFP were combined with Lipofectamine 2000 (Gibco-BRL) for transfection. Recordings were made 48 h after transfection.

Single-Channel Recordings. Coverslips containing cells were removed from the incubator before experiments and placed in a chamber (250-μL volume) containing the control bath solution at room temperature (20–22 °C). Single-channel currents were recorded in the cell-attached patch configuration with an Axopatch 200B patch clamp amplifier and pClamp 10 software (Molecular Devices Inc.). Patch electrodes were fabricated using thin-walled borosilicate glass (World Precision Instruments) and coated with Sylgard (Dow Corning). Electrodes had a resistance measured with recording solutions of ~10–25 MΩ. The patch pipettes contained (in mM) 135 NaCl, 5 KCl, 10 Hepes, 1 $MgCl_2$, 1 $CaCl_2$ and was adjusted to pH 7.4 with NaOH. The bath solution contained (in mM) 135 KCl, 1 $MgCl_2$, 1 $CaCl_2$, 10 Hepes and was adjusted to pH 7.4 with KOH. At acquisition the single-channel currents were low-pass filtered at 2 kHz (−3dB, four-pole Bessel filter) and sampled at 10 kHz. No junction potential correction was done on data acquired in the cell-attached recording.

Data Analysis. Single-channel records were analyzed with Clampfit 10 (Molecular Devices, Inc.) after digital filtering between 1,000 and 200 Hz. Capacitive currents were removed by subtracting the average of sweeps obtained at the same voltage that showed no channel activity (i.e., blank or null sweeps). Given a combined analog and digital filter frequency of 199 Hz (f_c), the rise time (T_r) of the system was calculated to be 1.7 ms using the equation $T_r = 0.332/f_c$, and the dead time (T_d) was calculated as $0.54 \times T_r$ = 0.9 ms (27). Half-amplitude threshold analysis (27) was used to detect events and generate idealized records from which dwell-time histograms and ensemble time courses were constructed. Events with durations shorter than 2 T_d were not included in exponential fits of dwell times, and events with durations shorter than 2 T_r were excluded from amplitude histograms. Only openings from single channels were analyzed for kinetics, but corrections were applied for Po (49) and first latency (50) in patches with evidence of more than one channel. The choice of the number of components used for fitting was based on a maximum-likelihood technique in which the least number of components with a significant improvement was used. For subconductance analysis, data were analyzed multiple times by two independent observers to ensure accurate event idealization. Data are expressed as mean ± SEM with the number of the cells (n) ≥ 5, unless otherwise stated. Single-channel records were filtered at 200 Hz for presentation in figures unless otherwise stated.

The Po values for 40, 60, and 80 mV were measured from patches estimated to have 1–3 channels, but the Po values for 0 and 20 mV are from patches with four or more channels so that enough events could be recorded. For each patch, the number of channels was estimated by dividing the maximum current reached at 60 mV by the mean open single-channel amplitude. Po then was corrected by dividing by the number of estimated channels.

Hidden Markov Model and Simulation. A Markov model was generated based on Silva and Rudy (3) and tested using QuB software [www.qub.buffalo.edu (51, 52)]. Rates for movement through the closed states in the activation pathway were calculated from Silva and Rudy for a membrane voltage of +60 mV. Adaptations then were made so that simulations of single-channel behavior fit better with experimental data. These adaptations included (*i*) the second closed transition states were converted to conducting states with amplitudes of 0.130, 0.196, 0.293, 0.440, and 0.660 pA; (*ii*) a C_f, state was added off each open state to account for the fast closings not produced by the existing model; (*iii*) the same rate constants were used between each open state (other than the more rarely visited 0.66-pA open state) to allow the channel to move back and forth between subconducting states instead of accumulating in the larger-amplitude conducting states. Rates for the transitions to/from all the open states in the vertical pathway were generated based on comparisons with experimental data, as were the rates to/from the C_f state. To generate simulated deactivation records, the main conducting level (0.44 pA) was selected as the start state, and all the original Silva and Rudy rates were recalculated for the step to −40 mV.

Simulated data were imported into pClamp10 for half-amplitude threshold analysis (27) to detect events and generate idealized records from which dwell-time histograms and ensemble time courses were constructed.

ACKNOWLEDGMENTS. We thank Kyung Hee Park for excellent technical assistance. This work was supported by grants from the Canadian Institutes of Health Research and the Heart and Stroke Foundation of British Columbia and Yukon (to D.F.).

1. Stengl M, et al. (2003) Accumulation of slowly activating delayed rectifier potassium current (IKs) in canine ventricular myocytes. *J Physiol* 551(Pt 3):777–786.
2. Jost N, et al. (2005) Restricting excessive cardiac action potential and QT prolongation: A vital role for IKs in human ventricular muscle. *Circulation* 112(10): 1392–1399.
3. Silva J, Rudy Y (2005) Subunit interaction determines IKs participation in cardiac repolarization and repolarization reserve. *Circulation* 112(10):1384–1391.
4. Sanguinetti MC, et al. (1996) Coassembly of $K_{(V)}$LQT1 and minK (IsK) proteins to form cardiac $I_{(Ks)}$ potassium channel. *Nature* 384(6604):80–83.
5. Barhanin J, et al. (1996) K(V)LQT1 and IsK (minK) proteins associate to form the I(Ks) cardiac potassium current. *Nature* 384(6604):78–80.
6. Wang Q, et al. (1996) Positional cloning of a novel potassium channel gene: *KVLQT1* mutations cause cardiac arrhythmias. *Nat Genet* 12(1):17–23.
7. Chen YH, et al. (2003) KCNQ1 gain-of-function mutation in familial atrial fibrillation. *Science* 299(5604):251–254.
8. Bellocq C, et al. (2004) Mutation in the KCNQ1 gene leading to the short QT-interval syndrome. *Circulation* 109(20):2394–2397.
9. Osteen JD, et al. (2010) KCNE1 alters the voltage sensor movements necessary to open the KCNQ1 channel gate. *Proc Natl Acad Sci USA* 107(52):22710–22715.
10. Zheng J, Sigworth FJ (1997) Selectivity changes during activation of mutant *Shaker* potassium channels. *J Gen Physiol* 110(2):101–117.
11. Chapman ML, VanDongen HMA, VanDongen AMJ (1997) Activation-dependent subconductance levels in the drk1 K channel suggest a subunit basis for ion permeation and gating. *Biophys J* 72(2 Pt 1):708–719.
12. Yang YS, Sigworth FJ (1998) Single-channel properties of I_{Ks} potassium channels. *J Gen Physiol* 112(6):665–678.
13. Romey G, et al. (1997) Molecular mechanism and functional significance of the MinK control of the KvLQT1 channel activity. *J Biol Chem* 272(27):16713–16716.
14. Sesti F, Goldstein SAN (1998) Single-channel characteristics of wild-type I_{Ks} channels and channels formed with two minK mutants that cause long QT syndrome. *J Gen Physiol* 112(6):651–663.
15. Pusch M (1998) Increase of the single-channel conductance of KvLQT1 potassium channels induced by the association with minK. *Pflugers Arch* 437(1):172–174.
16. Pusch M, Magrassi R, Wollnik B, Conti F (1998) Activation and inactivation of homomeric KvLQT1 potassium channels. *Biophys J* 75(2):785–792.
17. Chapman ML, VanDongen AMJ (2005) K channel subconductance levels result from heteromeric pore conformations. *J Gen Physiol* 126(2):87–103.
18. Zheng J, Sigworth FJ (1998) Intermediate conductances during deactivation of heteromultimeric Shaker potassium channels. *J Gen Physiol* 112(4):457–474.
19. Sanguinetti MC, Jurkiewicz NK (1990) Two components of delayed rectifier K^+ current. *J Gen Physiol* 96:195–215.
20. Seebohm G, et al. (2001) A kinetic study on the stereospecific inhibition of KCNQ1 and I(Ks) by the chromanol 293B. *Br J Pharmacol* 134(8):1647–1654.

21. Lerche C, et al. (2007) Chromanol 293B binding in KCNQ1 (Kv7.1) channels involves electrostatic interactions with a potassium ion in the selectivity filter. *Mol Pharmacol* 71(6):1503–1511.
22. Busch AE, et al. (1996) Inhibition of IKs in guinea pig cardiac myocytes and guinea pig IsK channels by the chromanol 293B. *Pflugers Arch* 432(6):1094–1096.
23. Imredy JP, Penniman JR, Dech SJ, Irving WD, Salata JJ (2008) Modeling of the adrenergic response of the human IKs current (hKCNQ1/hKCNE1) stably expressed in HEK-293 cells. *Am J Physiol Heart Circ Physiol* 295(5):H1867–H1881.
24. Nakajo K, Ulbrich MH, Kubo Y, Isacoff EY (2010) Stoichiometry of the KCNQ1 - KCNE1 ion channel complex. *Proc Natl Acad Sci USA* 107(44):18862–18867.
25. Eldstrom J, et al. (2010) Mechanistic basis for LQT1 caused by S3 mutations in the KCNQ1 subunit of IKs. *J Gen Physiol* 135(5):433–448.
26. Tzounopoulos T, Maylie J, Adelman JP (1998) Gating of I(sK) channels expressed in Xenopus oocytes. *Biophys J* 74(5):2299–2305.
27. Colquhoun D, Sigworth FJ (1995) *Single-Channel Recording*, eds Sakmann B, Neher E (Plenum, New York), pp 483–587.
28. Tyerman SD, Terry BR, Findlay GP (1992) Multiple conductances in the large K+ channel from Chara corallina shown by a transient analysis method. *Biophys J* 61(3): 736–749.
29. Pollard JR, Arispe N, Rojas E, Pollard HB (1994) A geometric sequence that accurately describes allowed multiple conductance levels of ion channels: the "three-halves (3/2) rule". *Biophys J* 67(2):647–655.
30. Qin F (2004) Restoration of single-channel currents using the segmental k-means method based on hidden Markov modeling. *Biophys J* 86(3):1488–1501.
31. Restier L, Cheng L, Sanguinetti MC (2008) Mechanisms by which atrial fibrillation-associated mutations in the S1 domain of KCNQ1 slow deactivation of I(Ks) channels. *Journal of Physiology-London* 586(Pt 17):4179–4191.
32. Hoshi T, Zagotta WN, Aldrich RW (1994) *Shaker* potassium channel gating. I: Transitions near the open state. *J Gen Physiol* 103(2):249–278.
33. Ma LJ, Ohmert I, Vardanyan V (2011) Allosteric features of KCNQ1 gating revealed by alanine scanning mutagenesis. *Biophys J* 100(4):885–894.
34. Osteen JD, et al. (2012) Allosteric gating mechanism underlies the flexible gating of KCNQ1 potassium channels. *Proc Natl Acad Sci USA* 109(18):7103–7108.
35. Zhou JY, Potts JF, Trimmer JS, Agnew WS, Sigworth FJ (1991) Multiple gating modes and the effect of modulating factors on the microI sodium channel. *Neuron* 7(5): 775–785.
36. Yue DT, Herzig S, Marban E (1990) Beta-adrenergic stimulation of calcium channels occurs by potentiation of high-activity gating modes. *Proc Natl Acad Sci USA* 87(2): 753–757.
37. Loussouarn G, et al. (2003) Phosphatidylinositol-4,5-bisphosphate, PIP2, controls KCNQ1/KCNE1 voltage-gated potassium channels: A functional homology between voltage-gated and inward rectifier K+ channels. *EMBO J* 22(20):5412–5421.
38. Marx SO, et al. (2002) Requirement of a macromolecular signaling complex for beta adrenergic receptor modulation of the KCNQ1-KCNE1 potassium channel. *Science* 295(5554):496–499.
39. Li Y, et al. (2011) KCNE1 enhances phosphatidylinositol 4,5-bisphosphate (PIP2) sensitivity of IKs to modulate channel activity. *Proc Natl Acad Sci USA* 108(22): 9095–9100.
40. Shamgar L, et al. (2006) Calmodulin is essential for cardiac IKS channel gating and assembly: Impaired function in long-QT mutations. *Circ Res* 98(8):1055–1063.
41. Volders PG, et al. (2003) Probing the contribution of IKs to canine ventricular repolarization: Key role for beta-adrenergic receptor stimulation. *Circulation* 107(21): 2753–2760.
42. Schoppa NE, Sigworth FJ (1998) Activation of *shaker* potassium channels. I. Characterization of voltage-dependent transitions. *J Gen Physiol* 111(2):271–294.
43. Choe H, Sackin H, Palmer LG (2001) Gating properties of inward-rectifier potassium channels: Effects of permeant ions. *J Membr Biol* 184(1):81–89.
44. Blunck R, McGuire H, Hyde HC, Bezanilla F (2008) Fluorescence detection of the movement of single KcsA subunits reveals cooperativity. *Proc Natl Acad Sci USA* 105(51):20263–20268.
45. Fox JA (1987) Ion channel subconductance states. *J Membr Biol* 97(1):1–8.
46. Zagotta WN, Hoshi T, Aldrich RW (1994) *Shaker* potassium channel gating. III: Evaluation of kinetic models for activation. *J Gen Physiol* 103(2):321–362.
47. Schoppa NE, Sigworth FJ (1998) Activation of *Shaker* potassium channels. III. An activation gating model for wild-type and V2 mutant channels. *J Gen Physiol* 111(2): 313–342.
48. Suh BC, Inoue T, Meyer T, Hille B (2006) Rapid chemically induced changes of PtdIns (4,5)P2 gate KCNQ ion channels. *Science* 314(5804):1454–1457.
49. Colquhoun D, Hawkes AG (1990) Stochastic properties of ion channel openings and bursts in a membrane patch that contains two channels: Evidence concerning the number of channels present when a record containing only single openings is observed. *Proc R Soc Lond B Biol Sci* 240(1299):453–477.
50. Aldrich RW, Corey DP, Stevens CF (1983) A reinterpretation of mammalian sodium channel gating based on single channel recording. *Nature* 306(5942):436–441.
51. Qin F, Auerbach A, Sachs F (1996) Estimating single-channel kinetic parameters from idealized patch-clamp data containing missed events. *Biophys J* 70(1):264–280.
52. Qin F, Auerbach A, Sachs F (2000) A direct optimization approach to hidden Markov modeling for single channel kinetics. *Biophys J* 79(4):1915–1927.